AGU PUBLICATIONS

Geophysical Research Letters

RESEARCH LETTER
10.1002/2014GL059816

Key Points:
- Measurable topologic symmetry is ingrained in the structure of channel networks
- The degree of symmetry distinguishes random networks from natural ones
- The symmetry is diagnostic of the process that shapes the network

Supporting Information:
- readme.pdf
- Text S1, Figures S1–S9, and Tables S1 and S2

Correspondence to:
E. Shelef,
shelef@stanford.edu

Citation:
Shelef, E., and G. E. Hilley (2014), Symmetry, randomness, and process in the structure of branched channel networks, *Geophys. Res. Lett.*, *41*, 3485–3493, doi:10.1002/2014GL059816.

Received 4 MAR 2014
Accepted 29 APR 2014
Accepted article online 3 MAY 2014
Published online 22 MAY 2014

Symmetry, randomness, and process in the structure of branched channel networks

Eitan Shelef[1] and George E. Hilley[1]

[1]Department of Geological and Environmental Sciences, Stanford University, Stanford, CA, USA

Abstract The branched structure of channel networks has a primary impact on the spatial distribution of elevation, water, and life across Earth's surface from the hillslope to the continental scale and is also observed on other planets. However, the link between this dendritic multiscale structure and the erosional processes that sculpt it has remained elusive for more than six decades. In fact, many topologic measures fail to distinguish natural networks from those generated by random walks. Here we show that a fundamental multiscale topologic symmetry is ingrained into the structure of these networks and reflects the equal elevation drop spanned by flows that split at the drainage divide and meet again downslope. We demonstrate that this symmetry distinguishes random-walk networks from natural ones, captures the temporal evolution of these networks, and divulges information about the processes that shape them.

1. Introduction

The pervasiveness of and order within the structure of Branched Channel Networks (BCNs) fueled some of the earliest interest in landscape forms [*Playfair*, 1802; *Gilbert*, 1877], but *Horton* [1945], was the first to relate metrics of this structure to the details of erosional mechanics in operation within drainage basins. Horton's theory, which linked metrics of basin topology to the action of fluvial erosion, was challenged by *Leopold and Langbein* [1962], who postulated that BCNs are structured to maximize entropy in a geomorphic system, regardless of the details of erosional mechanics. They found that a random-walk process (Figure 1a) produces network topologies indistinguishable from those observed in nature when Horton's metrics were used to quantify their form. Their results were later corroborated by *Shreve* [1966]. Interestingly, these topologic consistencies were also measured over demonstrably nonrandom networks, constrained by criteria of slope [*Howard*, 1971], energy optimization [*Howard*, 1990; *Rodríguez-Iturbe et al.*, 1992], hypothesized landshaping processes [*Leheny and Nagel*, 1993], or strict topological attributes [*Kirchner*, 1993], thus culminating in the conclusion that the plan view topology of BCNs produces similar Horton's metrics regardless of how they form [*Kirchner*, 1993]. This conclusion was later challenged through investigations of networks simulated using a minimum energy expenditure hypothesis [i.e., *Rodríguez-Iturbe et al.*, 1992], which demonstrated that Horton's metrics are avoidable, and that natural, simulated, and random-walk networks can be distinguished through simultaneous comparison of multiple plan view metrics that primarily rely on basin's length and drainage area [*Rigon et al.*, 1993; *Rodríguez-Iturbe and Rinaldo*, 1997; *Rinaldo et al.*, 1998, 2014].

An alternative approach to understanding landscape form uses conservation of mass with semiempirical Geomorphic Transport Laws [*Dietrich et al.*, 2003] to produce Landscape Evolution Models (LEMs) that predict topographic evolution [*Willgoose et al.*, 1991a; *Howard*, 1994; *Perron et al.*, 2012]. LEMs produce topography that is continuous across the model domain as it evolves to a steady state form in which mass inputs to a landscape are balanced by erosional mass export (Figure 1d). This approach prove useful in exploring landscape temporal evolution and response to different processes and external conditions [*Willgoose et al.*, 1991a; *Howard*, 1994; *Dietrich et al.*, 2003; *Perron et al.*, 2009]. However, until recently [*Perron et al.*, 2012; *Willett et al.*, 2014], no studies have been able to explicitly link plan view attributes of BCNs directly to the erosional mechanics that operate within them. The studies that made this link did so either at the uppermost tips of BCNs where hillslopes transition to channels [*Perron et al.*, 2012], or to explore the impact of BCNs configuration on processes of divide migration [*Willett et al.*, 2014]. Hence, it is still unclear how the details of erosional mechanics impact the multiscale geometry of an entire network [*Leopold and Langbein*, 1962; *Shreve*, 1966; *Dietrich and Montgomery*, 1998; *Rinaldo et al.*, 1998; *Dodds and Rothman*, 2000].

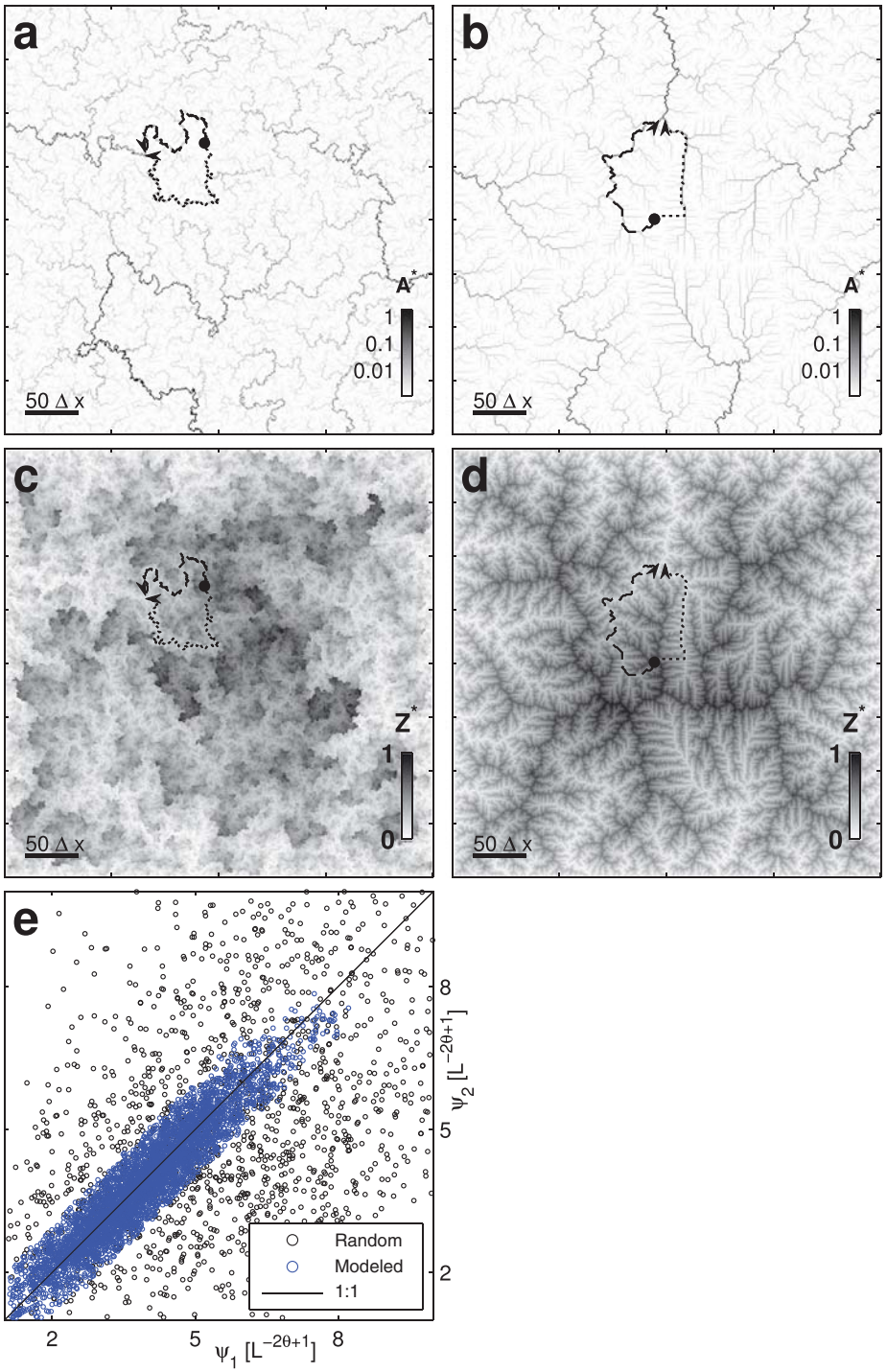

Figure 1. Detection of topographic discontinuities using ψ. Drainage area map (normalized to maximum watershed area; A^*) of (a) random-walk and (b) modeled (i.e., LEM-produced with specified $\theta = 0.5$. Table S1) networks. Dashed and dotted arrows mark example paired flow paths. (c,d) Elevations (normalized to maximum elevation; Z^*) calculated from the area maps by upslope integration of equation (2) from the fixed elevation boundaries with $\theta = 0.5$. Random-walk network configurations, shown in Figure 1c, produce sharp elevation discontinuities across divides because flow paths are not necessarily configured to abide by equation (3). (e) ψ_1 versus ψ_2 for all paired-flows of $\psi \leq 10$ within these random and modeled landscapes. ψ_1 and ψ_2 are arbitrarily assigned to visualize the scatter around the 1:1 line that denotes $\psi_1 = \psi_2$.

This contribution addresses the link between channel forming processes and the multiscale geometry of BCNs. We use the methodology detailed below to show that the structure of BCNs is constrained by a multiscale topologic symmetry that distinguishes random-walk networks from natural and simulated ones. We then show that this symmetry captures the temporal evolution of BCNs topology, and links the geometry of the entire channel network to the processes that form it (as captured by the channel profile) and to the degree by which these processes modify preexisting topography.

2. Method

We draw on the geometry of the channel profile to define a process-related constraint on the branched plan view structure of BCNs. When a landscape is at steady state, so that incision is everywhere balanced by rock uplift, the along-flow profile of channels is concave up so that channel slope (S[]) and drainage area (A[L^2]) are related to one another as [*Howard*, 1971; *Howard and Kerby*, 1983; *Willgoose et al.*, 1991b]

$$S \propto A^{-\theta} , \tag{1}$$

where θ, the channel concavity, is empirically dependent on the channel forming process and likely reflects the process mechanics [*Willgoose et al.*, 1991b; *Seidl and Dietrich*, 1992; *Whipple and Tucker*, 1999; *Whipple et al.*, 2000; *Tucker and Whipple*, 2002; *Mitchell*, 2005; *Stock and Dietrich*, 2006]. Thus, the elevation drop (Δz [L]) between two points along a channel at steady state is dependent on θ and on the distribution of drainage areas along the distance (L_f [L]) between these two points [e.g., *Perron and Royden*, 2012; *Willett et al.*, 2014]:

$$\Delta z \propto \int_0^{L_f} A(L)^{-\theta} \mathrm{d}L, \tag{2}$$

where $A(L)$ acknowledges that drainage area changes along the channel length (L). Finally, we utilize the fact that flow paths that initiate at an infinitesimal distance apart on each side of a continuous drainage divide and rejoin downslope (Figures 1a–1d) must share the same elevation drop along their flow route. For simplicity we assume that the extent and relief of hillslopes is negligible compared to that of these paired flow paths and that the proportionality constant between S and $A^{-\theta}$ is everywhere constant. In that case, the symmetry in elevation drop across the divide implies

$$\int_0^{L_{f1}} A_1(L)^{-\theta} \mathrm{d}L \simeq \int_0^{L_{f2}} A_2(L)^{-\theta} \mathrm{d}L , \tag{3}$$

where the right-hand side and left-hand side represent the proportionate elevation drop (ψ[L$^{-2\theta+1}$]) between divide and junction along two flow paths (noted as subscripts 1 and 2). Thus, the channel concavity (θ) and the arrangement of drainage areas in the watershed determines the three-dimensional basin topography such that it ensures a symmetry in ψ across divides (i.e., equation (3)) of various scales. The arrangement of basin areas is produced by the network topology, and so this topology must be configured in accordance with θ such that it satisfies this symmetry everywhere across the landscape.

This simple analysis suggests that the adherence of a network to the symmetry constraints required by equation (3) can be measured using the discordance between the proportionate elevation drops (ψ_1, ψ_2) along sets of flow paths initiating and rejoining at each divide and junction in a network, respectively. Our procedure for assessing consistency of a BCN's geometry with its three-dimensional structure identifies all paired flow paths that initiate at adjacent points along each drainage divide in the landscape and traverse the same junction, and calculates a discrete form of ψ for each one of these flows

$$\psi = \sum_i^{n_p} A_i^{-\theta} \Delta l_i , \tag{4}$$

where n_p is the number of nodes along the flow pathway, A_i is the drainage area of the ith node, and Δl_i is the distance between the ith node and its down-flow neighbor. We then quantify the consistency of ψ_1 and ψ_2 with equation (3). Basins in which paired flow paths are configured to satisfy equation (3) can be visually identified by plotting ψ_1 versus ψ_2 and comparing the distribution of all pairs to the expected 1:1 line (Figure 1e). We calculated the basin-wide consistency of ψ_1 and ψ_2 pairs with equation (3) by a metric

$$C_n = \overline{\psi_{12}}^{-1} \sqrt{\left(\frac{1}{n_\psi} \sum_{i=1}^{n_\psi} \left(\psi_{1i} - \psi_{2i} \right)^2 \right)} , \tag{5}$$

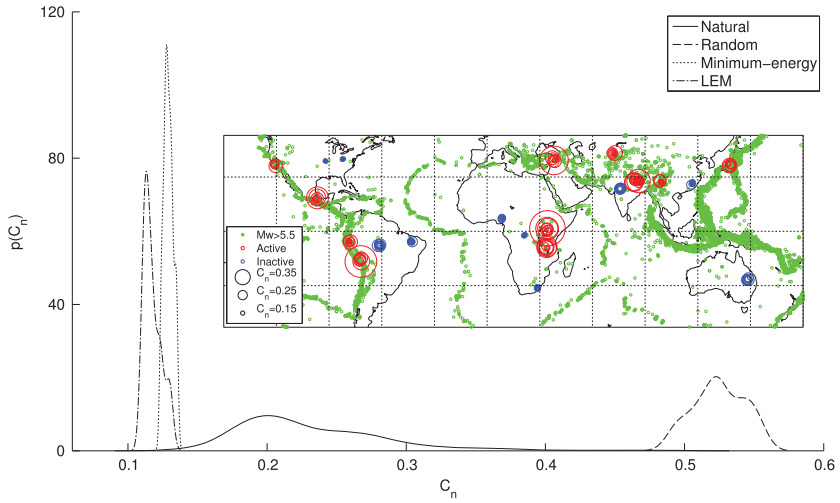

Figure 2. BCNs comparison. Probability density functions (PDFs) of C_n (x axis) calculated for natural (Table S2, $N = 207$), random-walk ($N = 140$), LEM networks ($N = 140$), and networks produced by minimizing energy expenditure ($N = 140$). C_n for each network is calculated from 10^2 to 10^4 sets of ψ_1, ψ_2 values. Inset map shows locations of analyzed natural networks extracted from SRTM90 DEMs [*Jarvis et al.*, 2008] super posited on an earthquake map (http://earthquake.usgs.gov/earthquakes). Circle size is proportional to C_n and red and blue circles mark C_n values for BCNs selected in seismically active and inactive areas, respectively. These two C_n populations are statistically distinct based on a Kolmogorov-Smirnov test ($\alpha = 0.99$). The empirical CDFs that underlie the PDFs plotted here (which were smoothed for better visualization using a normal kernel density estimator) are shown in Figure S1.

that reflects the ratio between the standard deviation of the difference between ψ_1 and ψ_2 around the expected zero, and the mean ψ value ($\overline{\psi_{12}}$) calculated for all ψ pairs across the basin (n_ψ). A minimal value of $C_n = 0$ reflects a perfect symmetry in ψ across divides (i.e., $\psi_1 = \psi_2$) everywhere in the basin.

We first performed this procedure over random-walk-generated, modeled, and natural BCNs to identify those network topologies that are inconsistent with the continuous topography and power law scaling of watershed area and channel slope typical of steady state landscapes. We then used this procedure to explore whether this symmetry captures the temporal evolution of BCNs topology over simulated landscape. Finally, we examined simulated BCNs of different concavities and show that the symmetry we propose explains plan view differences in the configuration of these networks, and the degree to which they modify preexisting topography.

3. Results

3.1. Comparison of Random-Walk-Generated, Modeled, and Natural BCNs

To explore whether the symmetry in ψ differentiates between BCNs produced by different procedures, we analyzed BCNs generated by random-walk-processes, LEMs, energy-minimization procedures, as well as those extracted from natural landscapes. We first generated random walk networks, akin to those produced by Leopold and Langbein [*Leopold and Langbein*, 1962] (Figure 1a). From these network topologies we then calculated watershed area and assumed a value of θ to calculate ψ_1 and ψ_2 for each set of paired flows (e.g., Figure 1e). An example random-walk simulation produces large misfits between ψ_1 and ψ_2 (Figures 1a, 1c, and 1e), which implies that topographic discontinuities are required by this network configuration and equation (1) (Figure 1c). The procedure was repeated for all random-walk networks to calculate probability densities of C_n (Figure 2)—all of these networks produced C_n values > 0.48 with $\theta = 0.5$ (varying θ between 0 and 1 did not significantly affect the results). Networks produced using the LEM [e.g., *Howard*, 1994; *Perron et al.*, 2009] and minimum energy expenditure methods [*Rodríguez-Iturbe et al.*, 1992; *Sun et al.*, 1994a] (both generated using specified values of $\theta = 0.5$, supporting information) all produced C_n values < 0.15. Finally, we performed the analysis procedure on 207 natural basins across the globe (Figure 2 in the supporting information). For each natural basin we calculated channel slopes and areas by routing flow over a 90 m Digital Elevation Model (DEM) and regressed over these slopes and areas to determine θ. We then used θ and the calculated areas to compute ψs and C_n (Figure 2, S2) as before and found mean C_n to be 0.23.

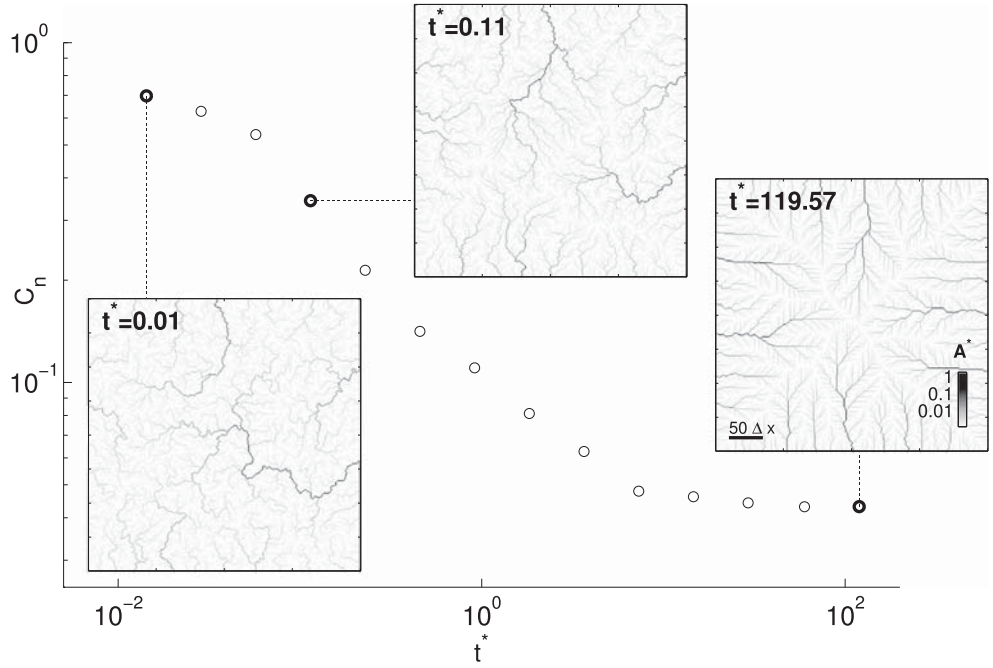

Figure 3. Transition of LEM-simulated networks from an initially disordered to an ordered state. Insets show normalized drainage area (A^*) maps for selected time steps (bold circles, connected via dotted lines). t^* (x axis) is dimensionless model time, calculated as $t^* = tU/z_m$, where t is model time and z_m is the steady state relief. Analysis is based on synthetic landscapes produced by LEM (Table S1), where θ is prescribed as 0.2 to highlight temporal differences in network configuration. The exact form of this curve depends on the initial and boundary conditions and on the concavity associated with the simulated channel forming process.

3.2. Temporal Reconfiguration of BCNs

We used LEM simulations to study the processes by which BCNs may transition from a disordered state in which $C_n \gg 0$ to one in which the network's form is balanced to maintain topographic continuity across the landscape ($C_n \simeq 0$). We designed a simple set of numerical experiments in which randomized initial topography was filled to prevent internal sinks, material was introduced into the model by uplift, all boundaries were held at fixed elevation during the simulation, and the topography was allowed to evolve through incision and sediment transport processes [e.g., *Howard*, 1994; *Pelletier*, 2004; *Perron et al.*, 2009](supporting information). Initially, the randomized, pit-filled initial topography produced networks of high C_n values that shared affinity to those produced by random walks (Figures 3 and S3). However, as the landscape evolved, the initially large misfits between ψ_1 and ψ_2 were removed, and the value of C_n decreased as the network progressively satisfied the symmetry required by equation (3)(Figures 3 and S3).

3.3. Channel Concavity and BCNs Configuration

The configuration of BCNs is dependent on the channel concavity [*Howard*, 1994; *Sun et al.*, 1994b; *Tucker and Whipple*, 2002]. To investigate the causes for this dependence and its link to the symmetry in ψ, we systematically changed θ in LEM simulations that share the same initial conditions and analyzed the resulting steady state BCNs configuration in comparison to their initial configuration. We calculated the correspondence between network geometries at the beginning and end of our LEM simulations using the cross correlation (C_c) between the drainage area maps of the initial and final time steps of each simulation (Figure 4):

$$C_c = \frac{\sum_{i=1}^{n_g} ({}^1A_i - {}^1\bar{A}_i) \times ({}^2A_i - {}^2\bar{A}_i)}{\sqrt{\sum_{i=1}^{n_g} ({}^1A_i - {}^1\bar{A}_i)^2} \times \sqrt{\sum_{i=1}^{n_g} ({}^2A_i - {}^2\bar{A}_i)^2}}, \quad (6)$$

where ${}^1A_i$, ${}^2A_i$ are the drainage areas of the ith's node of the two DEMs compared, ${}^1\bar{A}_i$, ${}^2\bar{A}_i$ are the mean drainage areas of these two landscapes, and n_g is the total number of nodes in each grid. C_c values of 1, −1, and 0 reflect perfect correlation, anticorrelation, and no correlation, respectively. C_c increased systematically from 0.08 to 0.89 when concavities changed between 0.1 and 0.8 (Figure 4a). This indicates that

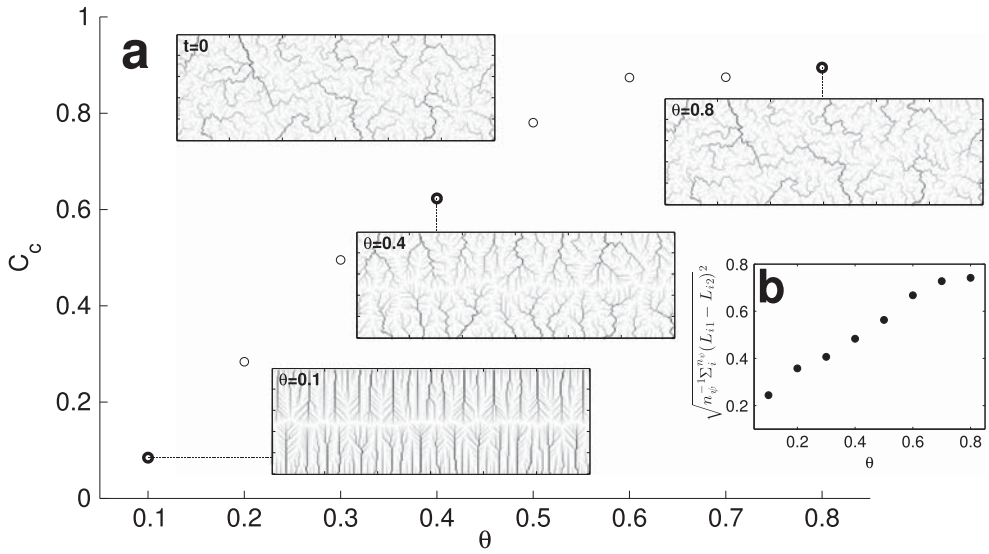

Figure 4. Impact of concavity on preservation of initial network structure. Simulation parameters presented in Table S1. (a) Cross-correlation (C_c, y axis) between drainage area maps of initial and steady state BCNs simulated with different concavities (θ, x axis). Insets show maps of normalized drainage area (A^*) for the initial ($t = 0$) configuration shared by all models, and for simulated landscapes with differing concavities after they evolved to a steady state form (connected via dotted lines to bold circles showing the C_c values of the associated concavity). (b) Relations between lengthwise symmetry (y-axis) and channel concavity (x axis). Lengthwise symmetry is quantified by the RMS of the difference between the flow pathway lengths of paired flows (L_1, L_2).

high-concavity landscapes systematically preserve the signature of preexisting topography as they evolve, while low-concavity landscapes tend to erase this signature.

The inset maps of Figure 4 demonstrate that low-θ networks show systematically higher degrees of plan view symmetry about drainage divides than their high-concavity counterparts that are tortuous and asymmetric. To investigate this similarity, we quantified the degree of lengthwise symmetry around drainage divides for these landscapes by calculating the difference in flow pathway lengths for each set of paired flows, and computing the root-mean-square of these differences (RMSD) for all paired flows in the simulated landscapes. These RMSD values increase from 0.24 to 0.74 as the concavity increases (Figure 4b) thus demonstrating that low-concavity networks are associated with higher degree of lengthwise symmetry around drainage divides.

We next used the symmetry in ψ to explore whether the network topology is diagnostic of the channel concavity. We used LEM-produced steady state landscapes simulated with concavities ranging from 0.2 to 0.7, and calculated C_n for each of these landscape using a range of concavity values ($\theta = 0$ to 0.8). When the concavity with which the landscape was simulated is ≤ 0.5, a minimal C_n value is attained when C_n is calculated using the same concavity with which the landscape was simulated (Figure S4). However, as the concavity of the simulated landscape increases, similarly low C_n values are also produced when the concavity used to calculate C_n is larger than the concavity with which the landscape is simulated.

4. Discussion

4.1. Symmetry in BCNs Produced by Random-Walk, Energy-Minimization, LEMs, and Natural Processes

The C_n values capture topologic differences between BCNs produced by different processes (Figure 2). The relatively high C_n values associated with random-walk-generated BCNs reflect the large misfits between ψ_1 and ψ_2 over such networks. These misfits demonstrate that C_n captures the simple fact that such networks are constructed regardless of a vertical dimension, so that their topology lacks the symmetry required to ensure equal elevation drop of paired flows whose θ values are similar to those observed in nature. In contrast to these high C_n values, networks produced via LEMs or energy-minimization procedures, produce distinctively lower C_n values (Figure 2) that reflect the topographic continuity of these landscapes. The small

difference in C_n between these landscapes may vary with the method used to attain and define the steady state configurations (Figure S6), and corroborates the proposed similarity of steady state solutions attained by the LEM and energy minimization approaches [*Sun et al.*, 1994b; *Sinclair and Ball*, 1996; *Banavar et al.*, 2001]. The C_n values of natural networks are lower than those of random ones but higher than those of simulated landscapes. These higher C_n values likely reflect deviations from equations (1) and (3) due to spatial variations in lithology, uplift and climate (Figure S7), as well as deviations from steady state conditions and the imprint of multiple geomorphic processes that are not accounted for in the simulated landscapes (Text S1 and Figures S4 and S5). This is demonstrated by the correlation between high C_n values and tectonically active areas (Figure 2), where such spatial heterogeneities and deviations from steady state are more likely to occur. Despite these natural heterogeneities, the probability density of C_n for natural networks overlaps with that of networks produced by LEMs and energy-minimization procedures, but is nonoverlapping with networks produced by a random-walk process (Figure 2). These findings firmly reject the hypothesis of *Leopold and Langbein* [1962] and demonstrate that the geometry of natural BCNs is poorly explained by random-walk processes but instead appears to more plausibly reflect the erosional processes within these watersheds as captured by equation (1).

4.2. Temporal Convergence to Symmetry

As demonstrated by Figures 3 and S3, initially large misfits between ψ_1 and ψ_2 were removed as the landscape evolved toward a steady state and the network topology progressively satisfied the symmetry required by equation (3). The transition between these states occurs through processes of divide migration [e.g., *Bishop*, 1986; *Mudd and Furbish*, 2005], where differences in slope across asymmetric divides cause differential erosion rates that lead to divide migration that continues until the slopes at each side of the divide are approximately equal. This process occurs over divides of basins of multiple scales where small basins equilibrate prior to larger ones (Figure S3), and so BCNs go through multiscale topologic reconfiguration that continues until all divides and ψ's approach symmetry.

4.3. Concavity, Process, and Network Configuration

The channel concavity (θ) probably reflects the mechanics of different erosional processes [e.g., *Willgoose et al.*, 1991b; *Seidl and Dietrich*, 1992; *Whipple and Tucker*, 1999; *Whipple et al.*, 2000; *Tucker and Whipple*, 2002; *Mitchell*, 2005; *Stock and Dietrich*, 2006]. For example, BCNs eroded by debris flows have demonstrably lower concavities than those dominated by fluvial processes [e.g., *Dietrich et al.*, 2003; *Stock and Dietrich*, 2003, 2006]. While the covariance between channel concavity and network configuration is typically attributed to boundary and initial conditions effects [e.g., *Howard*, 1994; *Tucker and Whipple*, 2002], an explicit link between these parameters remained elusive.

The symmetry in ψ provides such link and ties the channel concavity to the network configuration. The preservation of initial network configuration by high-concavity networks arises from the rapid increase in channel relief near the divides of such networks. This abrupt increase in relief allows large mismatches between ψ_1 and ψ_2 to be resolved with relatively little divide migration. Thus, as demonstrated in Figure 4, processes associated with high concavity may more readily preserve the initial form of networks than their low-concavity counterparts. A complementary explanation ties the geometric similarity between adjacent low-concavity BCNs (Figure 4) to the fact that as the value of θ decreases the symmetry in ψ develops into a lengthwise symmetry (i.e., equation (3) with $\theta \rightarrow 0$, Figure 4b) across divides (regardless if the paired flows meet at a junction or share an outlet at a boundary of common elevation). Such symmetry requires substantial changes in the initial configuration of BCNs and results in steady state topography of high visual similarity between adjacent basins. In contrast, very high θ values satisfy equation (3) regardless of the network configuration (i.e., equation (3) with $\theta \rightarrow \infty$) so that even a random-walk-like initial BCN configuration is preserved in the steady state topography (Figure 4a). Hence, transition from low- to high-concavity processes (e.g., from debris flows to detachment limited fluvial channels) will preserve the initial, low-concavity network configuration while an opposite transition may cause significant network reconfiguration. Thus, preexisting BCNs might serve as a template from which specific stable network configurations are ultimately selected, and the degree to which this template is modified may depend on the details of the erosional processes as captured by θ.

The topology of low-concavity networks is more diagnostic of their concavity than that of high-concavity networks, so that the concavity of simulated low-concavity channels ($\theta \leq 0.5$) can be computed from the network topology as captured by the spatial distribution of drainage areas (Figure S4). This difference

between low- and high-concavity networks likely reflects the relations between θ and the preservation of initial conditions (Figure 4), such that for $\theta > 0.5$ the initial conditions are well preserved and changes in θ has little influence on the degree of preservation (i.e., Figure 4, for $\theta > 0.5$). Thus, the configuration of simulated high-concavity networks primarily depends on the initial conditions and is less diagnostic of the value of θ. This suggests that the concavity of $\theta < 0.5$ networks can be reconstructed from plan view images when vertical data is not available (e.g., seismic images, Cassini Titan Radar Mapper images), and that the configuration of $\theta > 0.5$ networks divulges information regarding the initial topography from which the landscape was formed.

4.4. Method Limitations

While C_n and ψ provide convenient metrics to compare and analyze BCNs formed by different processes, the limitations of this methodology should be considered when applying it to landscape analysis. First, while $C_n = 0$ implies perfect symmetry, there is no finite C_n value that describes perfect asymmetry such that the interpretation of high C_n values is mostly comparative. The high C_n values calculated from random-walk networks ($C_n > 0.48$, mean $C_n = 0.52$, Figure 2) provide a convenient reference for such comparisons. Second, high C_n values may also arise from nonlinear relations between ψ_1 and ψ_2, or due to small number of ψ pairs that significantly deviate from a 1:1 line. Hence, detailed ψ-based interpretation requires analysis of ψ_1 vs. ψ_2 plots. Such detailed interpretation will also benefit from identifying the spatial location of ψ pairs that deviate from the general trend in these plots. Third, ψ-based landscape analysis relies on a homogeneous distribution of uplift, climate, lithology, and θ, so that high C_n values may reflect deviations from these assumption rather than, for example, deviations from steady state. In particular, this analysis does not account for the different θ values typically associated with hillslope and slope failure processes that may dominate small drainage area portions of the landscape. The effect of different θ at small drainage areas can be accounted for by calculating ψ from a paired flows junction up to a given area threshold [e.g., *Willett et al.*, 2014], or by using low-resolution DEMs where the extent of such processes is smaller than the DEM resolution. In cases where sufficient knowledge exists regarding the spatial distribution of θ, uplift, climate, and lithology, these spatial heterogeneities can be explicitly accounted for in the discrete calculation of ψ (i.e., equation (4)).

5. Summary

The multiscale plan view structure of BCNs reflects two coupled constraints: (a) the characteristic along-flow channel profile shaped by the channel forming processes (as reflected by the channel concavity; θ), and (b) the equal elevation drop spanned by two flows that initiate at an infinitesimal distance apart on each side of a drainage divide and meet again downslope. The coupling of these two constraints results in multiscale topological symmetry around drainage divides. We found that the degree to which these constraints are satisfied distinguishes random, natural, and modeled landscapes and captures differences in network configuration between tectonically active and inactive areas. We demonstrate that this topologic symmetry increases as the landscape approaches steady state and explains temporal variations in BCNs configuration. This symmetry also explains why simulated landscapes of various concavities differ in the degree of preservation of initial conditions, and in the topological similarity of adjacent basins. Thus, our findings demonstrate that preexisting BCNs might serve as a template from which specific stable network configurations are ultimately selected, and the degree to which this template is modified may depend on the details of the erosional processes as captured by the channel concavity (θ). Further work may use the approach proposed here to investigate spatiotemporal variations in these processes through their plan view topographic imprint and to reveal the mechanics of erosional processes on this and other planets.

Acknowledgements
Data supporting our LEM, energy-minimization, and random-walk networks production procedures and parameter values are available in Text S1, Figures S1–S9, and Table S1. SRTM90 DEM data used to extract natural networks are available through http://www.cgiar-csi.org/data/srtm-90m-digital-elevation-database-v4-1, and exact basin locations are specified in Table S2. We would like to thank Bayani Cardenas, Riccardo Rigon, and Efi Foufoula-Georgiou for insightful and thorough comments that helped improving this manuscript. We would also like to thank Taylor Perron for thoughtful comments on an earlier version of this manuscript. E.S. thanks the Lieberman Fellowship for its generous support.

The Editor thanks two anonymous reviewers for their assistance evaluating this paper.

References

Banavar, J. R., F. Colaiori, A. Flammini, A. Maritan, and A. Rinaldo (2001), Scaling, optimality, and landscape evolution, *J. Stat. Phys.*, *104*(1-2), 1–48.

Bishop, P. (1986), Horizontal stability of the australian continental drainage divide in south central New South Wales during the Cainozoic, *Aust. J. Earth Sci.*, *33*(3), 295–307.

Dietrich, W. E., and D. R. Montgomery (1998), Hillslopes, channels, and landscape scale, in *Scale Dependence and Scale Invariance in Hydrology*, edited by G. Sposito, pp. 30–60, Cambridge Univ. Press, Cambridge, U. K., doi:10.1017/CBO9780511551864.003.

Dietrich, W. E., D. G. Bellugi, L. S. Sklar, J. D. Stock, A. M. Heimsath, and J. J. Roering (2003), Geomorphic transport laws for predicting landscape form and dynamics, in *Geophys. Monogr. Ser.*, vol. 135, edited by P. Wilcock and R. Iverson, pp. 103–132, AGU, Washington, D. C., doi:10.1029/135GM09.

Dodds, P., and D. Rothman (2000), Scaling, universality, and geomorphology, *Annu. Rev. Earth Planet. Sci.*, *28*(1), 571–610, doi:10.1146/annurev.earth.28.1.571.
Gilbert, G. K. (1877), Report on the Geology of the Henry Mountains, in *U. S. Geographical and Geological Survey of the Rocky Mountain Region*, edited by J. W. Powell, pp. 170 p., Government Printing Office, Washington, D. C.
Horton, R. (1945), Erosional development of streams and their drainage basins; hydrophysical approach to quantitative morphology, *Geol. Soc. Am. Bull.*, *56*(3), 275–370.
Howard, A., and G. Kerby (1983), Channel changes in badlands, *Geol. Soc. Am. Bull.*, *94*(6), 739–752, doi:10.1130/0016-7606(1983)94<739:CCIB>2.0.CO;2.
Howard, A. D. (1971), Simulation model of stream capture, *Geol. Soc. Am. Bull.*, *82*(5), 1355–1376, doi:10.1130/0016-7606(1971)825B1355:SMOSC5D2.0.CO;2.
Howard, A. D. (1990), Theoretical model of optimal drainage networks, *Water Resour. Res.*, *26*(9), 2107–2117, doi:10.1029/WR026i009p02107.
Howard, A. D. (1994), A detachment-limited model of drainage basin evolution, *Water Resour. Res.*, *30*(7), 2261–2286, doi:10.1029/94WR00757.
Jarvis, A., H. Reuter, A. Nelson, and E. Guevara (2008), Hole-filled seamless SRTM data V4, International Centre for Tropical Agriculture (CIAT), Cali, Colombia. [Available at http://srtm.csi.cgiar.org.]
Kirchner, J. (1993), Statistical inevitability of Horton's laws and the apparent randomness of stream channel networks, *Geology*, *21*(7), 591–594, doi:10.1130/0091-7613(1993)021<0591:SIOHSL>2.3.CO;2.
Leheny, R. L., and S. R. Nagel (1993), Model for the evolution of river networks, *Phys. Rev. Lett.*, *71*(9), 1470–1473, doi:10.1103/PhysRevLett.71.1470.
Leopold, L., and W. Langbein (1962), The concept of entropy in landscape evolution, *Geol. Surv. Prof. Pap. 500-A*, United States Government Printing Office, Washington, D. C.
Mitchell, N. (2005), Interpreting long-profiles of canyons in the USA Atlantic continental slope, *Mar. Geol.*, *214*(1), 75–99, doi:10.1016/j.margeo.2004.09.005.
Mudd, S. M., and D. J. Furbish (2005), Lateral migration of hillcrests in response to channel incision in soil-mantled landscapes, *J. Geophys. Res.*, *110*, F04026, doi:10.1029/2005JF000313.
Pelletier, J. (2004), Persistent drainage migration in a numerical landscape evolution model, *Geophys. Res. Lett.*, *31*, L20501, doi:10.1029/2004GL020802.
Perron, J., J. Kirchner, and W. Dietrich (2009), Formation of evenly spaced ridges and valleys, *Nature*, *460*(7254), 502–505, doi:10.1038/nature08174.
Perron, J., P. Richardson, K. Ferrier, and M. Lapôtre (2012), The root of branching river networks, *Nature*, *492*(742), 100–103, doi:10.1038/nature11672.
Perron, J. T., and L. Royden (2012), An integral approach to bedrock river profile analysis, *Earth Surf. Processes Landforms*, *38*, 570–576, doi:10.1002/esp.3302.
Playfair, J. (1802), *Illustrations of the Huttonian Theory of the Earth*, Cadell and Davies, Edinburgh, U. K.
Rigon, R., A. Rinaldo, I. Rodriguez-Iturbe, R. L. Bras, and E. Ijjasz-Vasquez (1993), Optimal channel networks: A framework for the study of river basin morphology, *Water Resour. Res.*, *29*(6), 1635–1646.
Rinaldo, A., I. Rodriguez-Iturbe, and R. Rigon (1998), Channel networks, *Annu. Rev. Earth Planet. Sci.*, *26*(1), 289–327, doi:10.1146/annurev.earth.26.1.289.
Rinaldo, A., R. Rigon, J. R. Banavar, A. Maritan, and I. Rodriguez-Iturbe (2014), Evolution and selection of river networks: Statics, dynamics, and complexity, *PNAS*, *111*(7), 2417–2424, doi:10.1073/pnas.1322700111.
Rodríguez-Iturbe, I., and A. Rinaldo (1997), *Fractal River Basins: Chance and Self-Organization*, Cambridge Univ. Press, Cambridge, U. K.
Rodríguez-Iturbe, I., A. Rinaldo, R. Rigon, R. Bras, A. Marani, and E. Ijjász-Vásquez (1992), Energy dissipation, runoff production, and the three-dimensional structure of river basins, *Water Resour. Res.*, *28*(4), 1095–1103, doi:10.1029/91WR03034.
Seidl, M., and W. Dietrich (1992), The problem of channel erosion into bedrock, in *Functional Geomorphology: Landform Analysis and Models: Festschrift for Frank Ahnert*, vol. Catena Supplement 23, edited by K. Schmidt and J. de Ploey, pp. 101–124, Catena Verlag, Cremlingen, Germany.
Shreve, R. L. (1966), Statistical law of stream numbers, *J. Geol.*, *74*(1), 17–37.
Sinclair, K., and R. C. Ball (1996), Mechanism for global optimization of river networks from local erosion rules, *Phys. Rev. Lett.*, *76*(18), 3360–3363, doi:10.1103/PhysRevLett.76.3360.
Stock, J., and W. E. Dietrich (2003), Valley incision by debris flows: Evidence of a topographic signature, *Water Resour. Res.*, *39*(4), 1089, doi:10.1029/2001WR001057.
Stock, J. D., and W. E. Dietrich (2006), Erosion of steepland valleys by debris flows, *Geol. Soc. Am. Bull.*, *118*(9), 1125, doi:10.1130/B25902.1.
Sun, T., P. Meakin, and T. Jøssang (1994a), Minimum energy dissipation model for river basin geometry, *Phys. Rev. E*, *49*(6), 4865, doi:10.1103/PhysRevE.49.4865.
Sun, T., P. Meakin, and T. Jøssang (1994b), The topography of optimal drainage basins, *Water Resour. Res.*, *30*(9), 2599–2610, doi:10.1029/94WR01050.
Tucker, G., and K. Whipple (2002), Topographic outcomes predicted by stream erosion models: Sensitivity analysis and intermodel comparison, *J. Geophys. Res.*, *107*(B9), 2179, doi:10.1029/2001JB000162.
Whipple, K., and G. Tucker (1999), Dynamics of the stream-power river incision model: Implications for height limits of mountain ranges, landscape response timescales, and research needs, *J. Geophys. Res.*, *104*, 17,661–17,674, doi:10.1029/1999JB900120.
Whipple, K., G. Hancock, and R. Anderson (2000), River incision into bedrock: Mechanics and relative efficacy of plucking, abrasion, and cavitation, *Geol. Soc. Am. Bull.*, *112*(3), 490–503, doi:10.1130/0016-7606(2000)112<490:RIIBMA>2.0.CO;2.
Willett, S. D., S. W. McCoy, J. T. Perron, L. Goren, and C.-Y. Chen (2014), Dynamic reorganization of river basins, *Science*, *343*(6175), 765, doi:10.1126/science.1248765.
Willgoose, G., R. Bras, and I. Rodriguez-Iturbe (1991a), A coupled channel network growth and hillslope evolution model: 1. Theory, *Water Resour. Res.*, *27*(7), 1671–1684, doi:10.1029/91WR00935.
Willgoose, G., R. L. Bras, and I. Rodriguez-Iturbe (1991b), A physical explanation of an observed link area-slope relationship, *Water Resour. Res.*, *27*(7), 1697–1702, doi:10.1029/91WR00937.